Supporting Information

O-GalNAcylation of RANTES Improves Its Properties as an HIV-1 Entry Inhibitor

Xiaoyang Guan,[1, ‡] Patrick K. Chaffey,[1, ‡] Huan Chen,[2, ‡] Wei Feng,[3, ‡] Xiuli Wei,[4] Liu-Meng Yang,[2] Yuan Ruan,[1] Xinfeng Wang,[1] Kimberly B. Barosh,[1] Amy H. Tran,[1] Jaimie Zhu,[1] Wei Liang,[4] Yong-Tang Zheng,[2,*] Xu Wang,[3,*] Zhongping Tan,[1,*]

1 Department of Chemistry and Biochemistry and BioFrontiers Institute, University of Colorado, Boulder CO 80303, United States
2 Key Laboratory of Animal Models and Human Disease Mechanisms of Chinese Academy of Sciences/Key Laboratory of Bioactive Peptides of Yunnan Province, Kunming Institute of Zoology, Kunming Institute of Zoology, Chinese Academy of Sciences, Kunming 650223, China
3 Department of Chemistry & Biochemistry, Arizona State University, Tempe, AZ 85287, United States
4 Protein & Peptide Pharmaceutical Laboratory, Institute of Biophysics, Chinese Academy of Sciences, Beijing 100101, China

Table of Contents

I. LC-MS analysis of purified RANTES variants.

LC-MS was performed with C4 column under 0.3 ml/min with a linear gradient of 15% to 35% acetonitrile in water over 5 min.

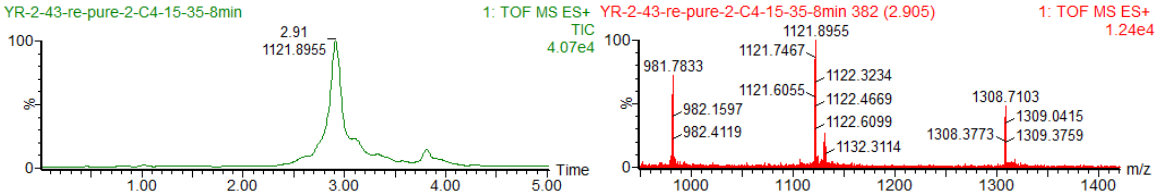

Figure S1-1. LC-MS traces and ESI-MS of RANTES analog **6**. MS (ESI) calculated for **6** $C_{350}H_{534}N_{96}O_{100}S_5$, Exact Mass: 7841.8255, $[M+6H]^{6+}$ m/z = 1307.9709 Da, $[M+7H]^{7+}$ m/z = 1121.2608 Da, $[M+8H]^{8+}$ m/z = 981.2282 Da.

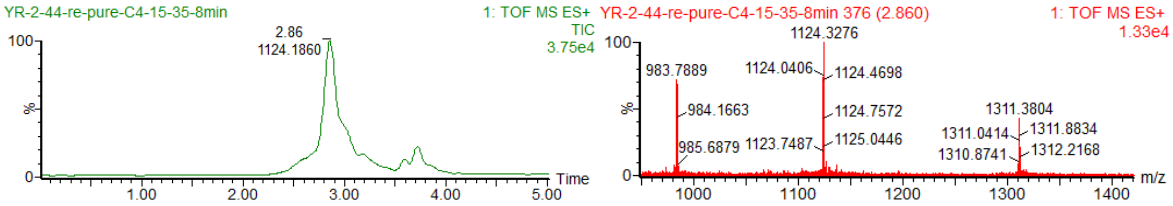

Figure S1-2. LC-MS traces and ESI-MS of RANTES analog **7**. MS (ESI) calculated for **7** $C_{350}H_{534}N_{96}O_{101}S_5$, Exact Mass: 7857.8204, $[M+6H]^{6+}$ m/z = 1310.6367 Da, $[M+7H]^{7+}$ m/z = 1123.5458 Da, $[M+8H]^{8+}$ m/z = 983.2276 Da.

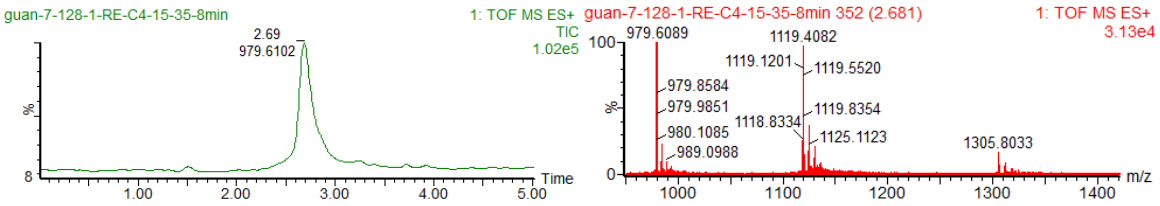

Figure S1-3. LC-MS traces and ESI-MS of RANTES analog **8**. MS (ESI) calculated for **8** $C_{351}H_{536}N_{96}O_{100}S_4$, Exact Mass: 7823.8691, $[M+6H]^{6+}$ m/z = 1304.9782 Da, $[M+7H]^{7+}$ m/z = 1118.6956 Da, $[M+8H]^{8+}$ m/z = 978.9836 Da.

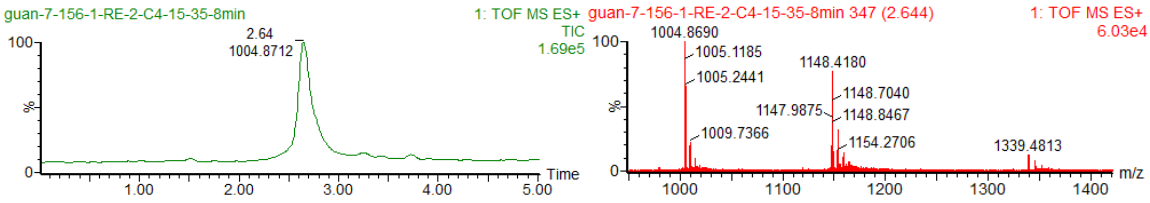

Figure S1-4. LC-MS traces and ESI-MS of RANTES analog **9**. MS (ESI) calculated for **9** $C_{359}H_{549}N_{97}O_{105}S_4$, Exact Mass: 8026.9484, $[M+6H]^{6+}$ m/z = 1338.8247 Da, $[M+7H]^{7+}$ m/z = 1147.7069 Da, $[M+8H]^{8+}$ m/z = 1004.3686 Da.

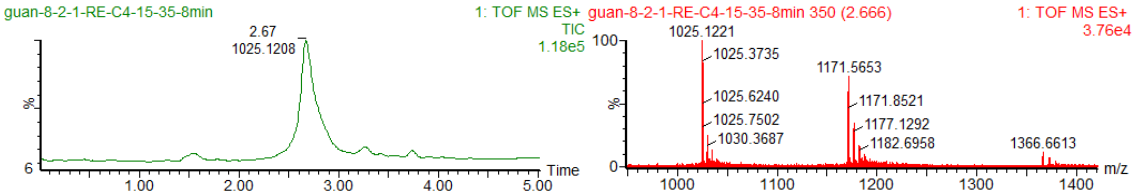

Figure S1-5. LC-MS traces and ESI-MS of RANTES analog **10**. MS (ESI) calculated for **10** $C_{365}H_{559}N_{97}O_{110}S_4$, Exact Mass: 8189.0013, $[M+6H]^{6+}$ m/z = 1365.8336 Da, $[M+7H]^{7+}$ m/z = 1170.8573 Da, $[M+8H]^{8+}$ m/z = 1024.6252 Da.

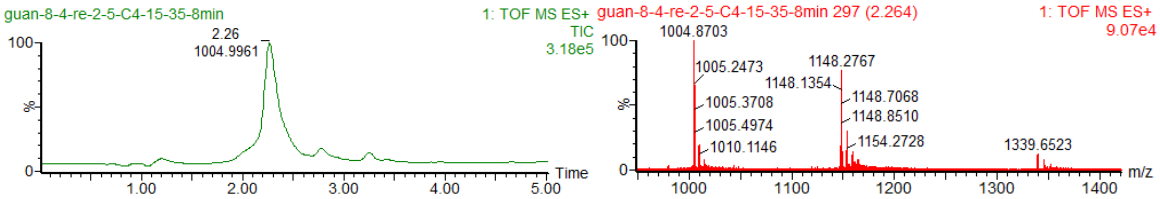

Figure S1-6. LC-MS traces and ESI-MS of RANTES analog **11**. MS (ESI) calculated for **11** $C_{359}H_{549}N_{97}O_{105}S_4$, Exact Mass: 8026.9484, $[M+6H]^{6+}$ m/z = 1338.8247 Da, $[M+7H]^{7+}$ m/z = 1147.7069 Da, $[M+8H]^{8+}$ m/z = 1004.3686 Da.

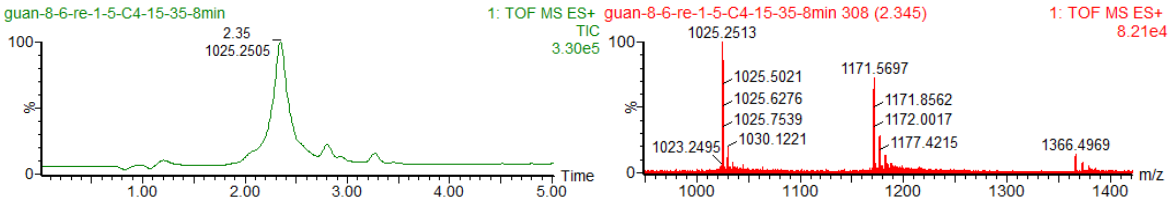

Figure S1-7. LC-MS traces and ESI-MS of RANTES analog **12**. MS (ESI) calculated for **12** $C_{365}H_{559}N_{97}O_{110}S_4$, Exact Mass: 8189.0013, $[M+6H]^{6+}$ m/z = 1365.8336 Da, $[M+7H]^{7+}$ m/z = 1170.8573 Da, $[M+8H]^{8+}$ m/z = 1024.6252 Da.

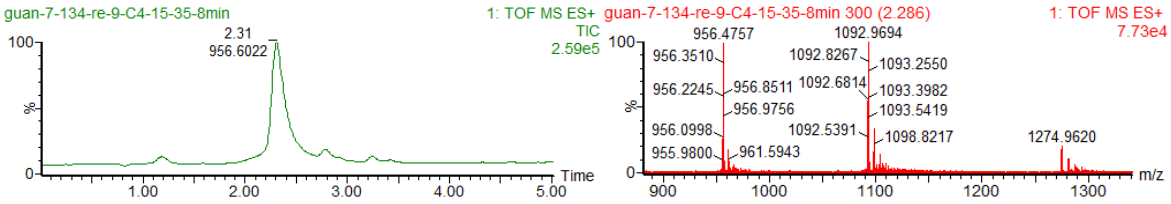

Figure S1-8. LC-MS traces and ESI-MS of RANTES analog **13**. MS (ESI) calculated for **13** $C_{343}H_{524}N_{94}O_{97}S_4$, Exact Mass: 7639.7843, $[M+6H]^{6+}$ m/z = 1274.2974 Da, $[M+7H]^{7+}$ m/z = 1092.3978 Da, $[M+8H]^{8+}$ m/z = 955.9730 Da.

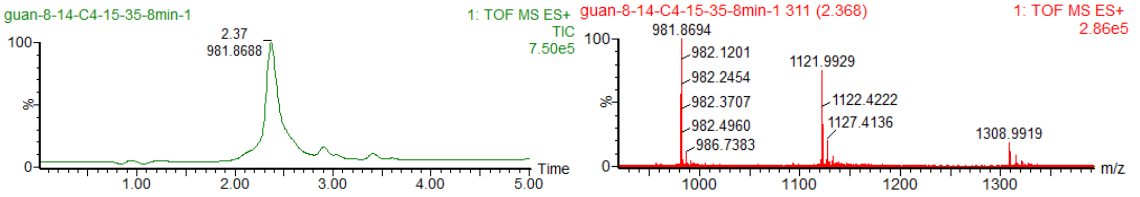

Figure S1-9. LC-MS traces and ESI-MS of RANTES analog **14**. MS (ESI) calculated for **14** $C_{351}H_{537}N_{95}O_{102}S_4$, Exact Mass: 7842.8636, $[M+6H]^{6+}$ m/z = 1308.1439 Da, $[M+7H]^{7+}$ m/z = 1121.4091 Da, $[M+8H]^{8+}$ m/z = 981.3580 Da.

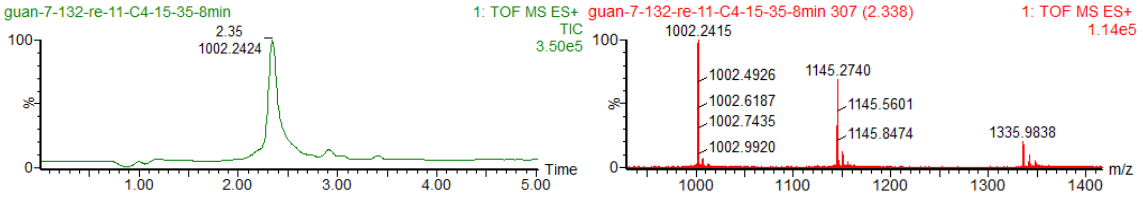

Figure S1-10. LC-MS traces and ESI-MS of RANTES analog **15**. MS (ESI) calculated for **15** $C_{357}H_{547}N_{95}O_{107}S_4$, Exact Mass: 8004.9165, $[M+6H]^{6+}$ m/z = 1335.1528 Da, $[M+7H]^{7+}$ m/z = 1144.5595 Da, $[M+8H]^{8+}$ m/z = 1001.6146 Da.

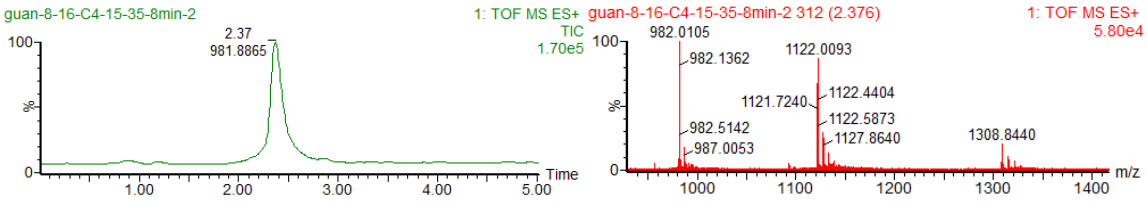

Figure S1-11. LC-MS traces and ESI-MS of RANTES analog **16**. MS (ESI) calculated for **16** $C_{351}H_{537}N_{95}O_{102}S_4$, Exact Mass: 7842.8636, $[M+6H]^{6+}$ m/z = 1308.1439 Da, $[M+7H]^{7+}$ m/z = 1121.4091 Da, $[M+8H]^{8+}$ m/z = 981.3580 Da.

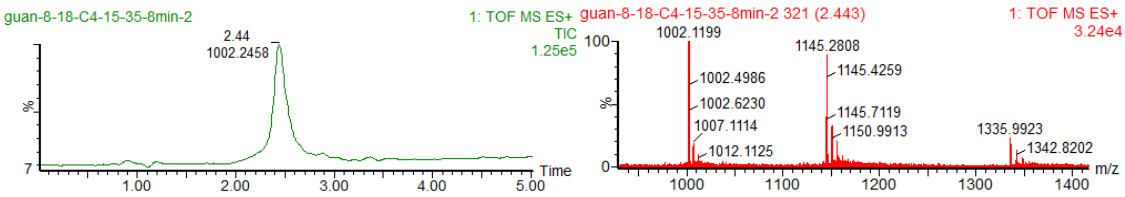

Figure S1-12. LC-MS traces and ESI-MS of RANTES analog **17**. MS (ESI) calculated for **17** $C_{357}H_{547}N_{95}O_{107}S_4$, Exact Mass: 8004.9165, $[M+6H]^{6+}$ m/z = 1335.1528 Da, $[M+7H]^{7+}$ m/z = 1144.5595 Da, $[M+8H]^{8+}$ m/z = 1001.6146 Da.

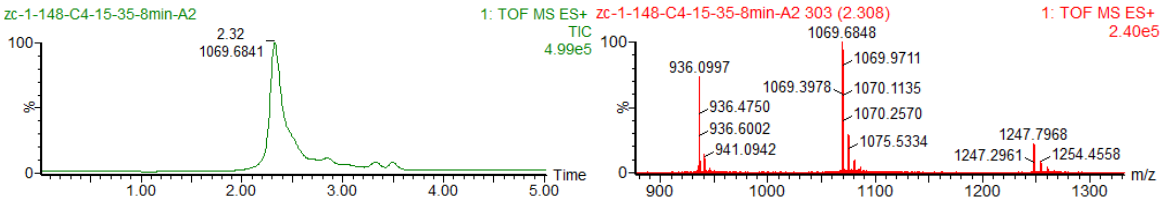

Figure S1-13. LC-MS traces and ESI-MS of RANTES analog **18**. MS (ESI) calculated for **18** $C_{334}H_{515}N_{93}O_{95}S_4$, Exact Mass: 7476.7209, $[M+6H]^{6+}$ m/z = 1247.1202 Da, $[M+7H]^{7+}$ m/z = 1069.1030 Da, $[M+8H]^{8+}$ m/z = 935.5901 Da.

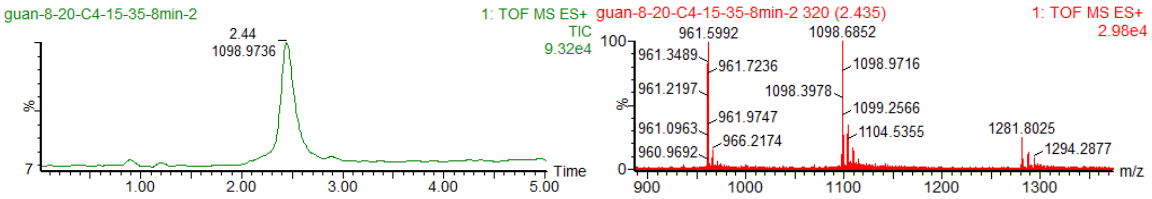

Figure S1-14. LC-MS traces and ESI-MS of RANTES analog **19**. MS (ESI) calculated for **19** $C_{342}H_{528}N_{94}O_{100}S_4$, Exact Mass: 7679.8003, $[M+6H]^{6+}$ m/z = 1280.9667 Da, $[M+7H]^{7+}$ m/z = 1098.1143 Da, $[M+8H]^{8+}$ m/z = 960.9750 Da.

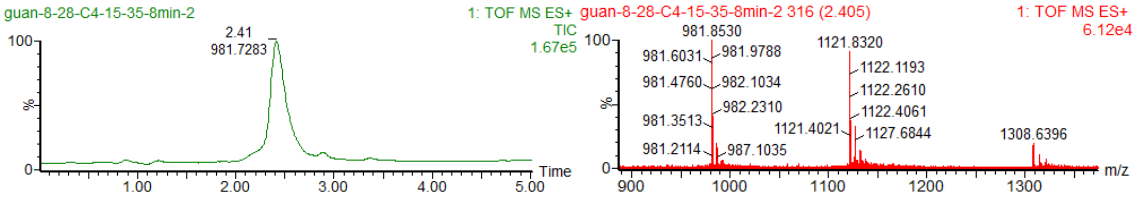

Figure S1-15. LC-MS traces and ESI-MS of RANTES analog **20**. MS (ESI) calculated for **20** $C_{348}H_{538}N_{94}O_{105}S_4$, Exact Mass: 7841.8531, $[M+6H]^{6+}$ m/z = 1307.9755 Da, $[M+7H]^{7+}$ m/z = 1121.2647 Da, $[M+8H]^{8+}$ m/z = 981.2316 Da.

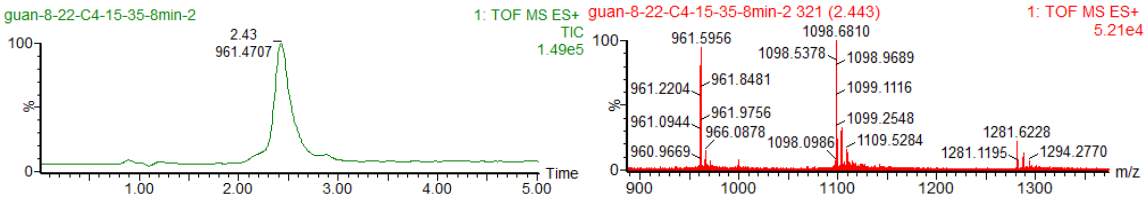

Figure S1-16. LC-MS traces and ESI-MS of RANTES analog **21**. MS (ESI) calculated for **21** $C_{342}H_{528}N_{94}O_{100}S_4$, Exact Mass: 7679.8003, $[M+6H]^{6+}$ m/z = 1280.9667 Da, $[M+7H]^{7+}$ m/z = 1098.1143 Da, $[M+8H]^{8+}$ m/z = 960.9750 Da.

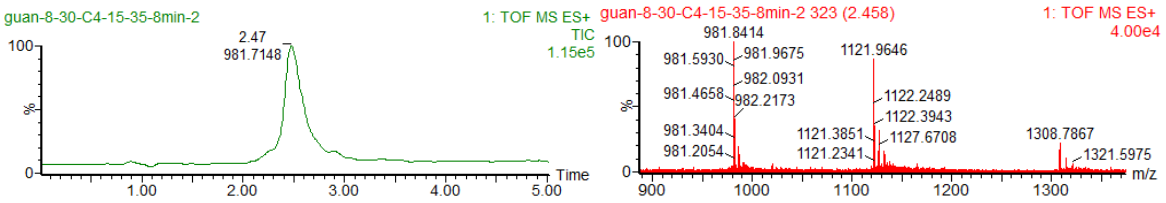

Figure S1-17. LC-MS traces and ESI-MS of RANTES analog **22**. MS (ESI) calculated for **22** $C_{348}H_{538}N_{94}O_{105}S_4$, Exact Mass: 7841.8531, $[M+6H]^{6+}$ m/z = 1307.9755 Da, $[M+7H]^{7+}$ m/z = 1121.2647 Da, $[M+8H]^{8+}$ m/z = 981.2316 Da.

II. Circular dichroism (CD) spectra of purified RANTES variants

The CD spectra were acquired in a 0.5 mm quartz cuvette under nitrogen at a flow rate of 1 L/min. Each peptide was dissolved in DPBS with peptide concentration as 0.2 g/L. CD spectra were obtained at 20 °C with a step of 0.5 nm, 0.5 s per point and a spectral width of 195-260 nm. The spectra are the average of 5 scans with an averaged 5 scan buffer baseline subtracted.

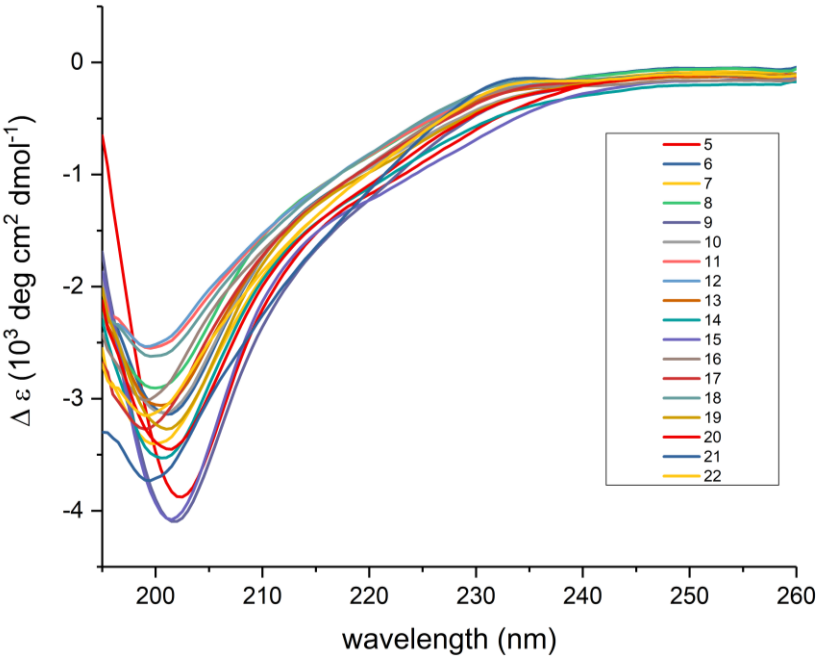

Figure S2-1. CD Spectra for all RANTES analogs.

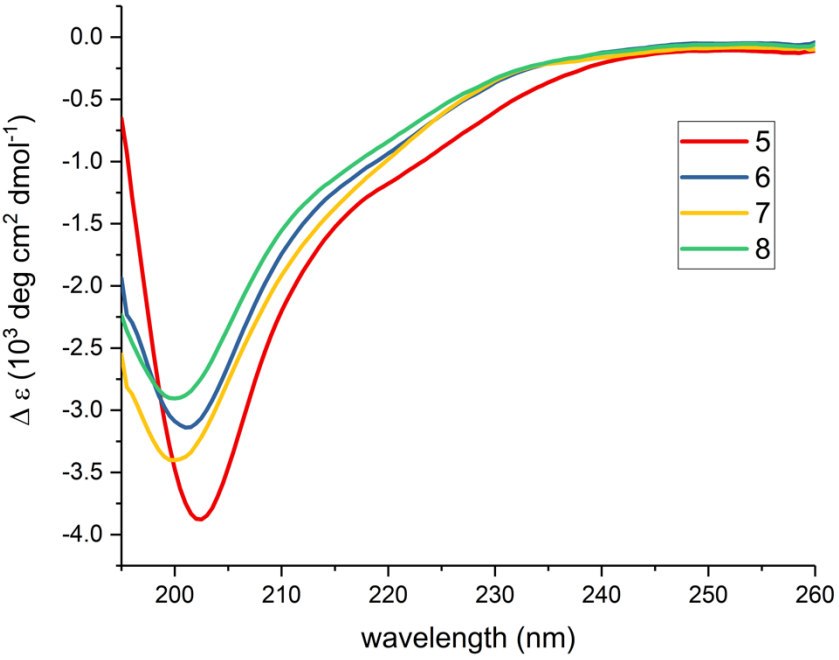

Figure S2-2. CD Spectra for Met67 mutant (1-68) RANTES analogs **5**-**8**.

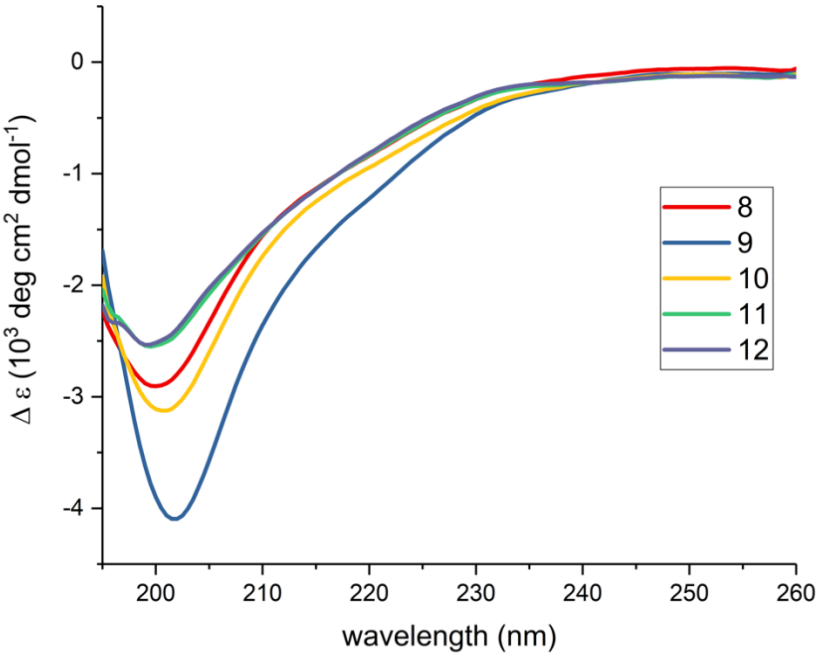

Figure S2-3. CD Spectra for (1-68) RANTES analogs **8**-**12**.

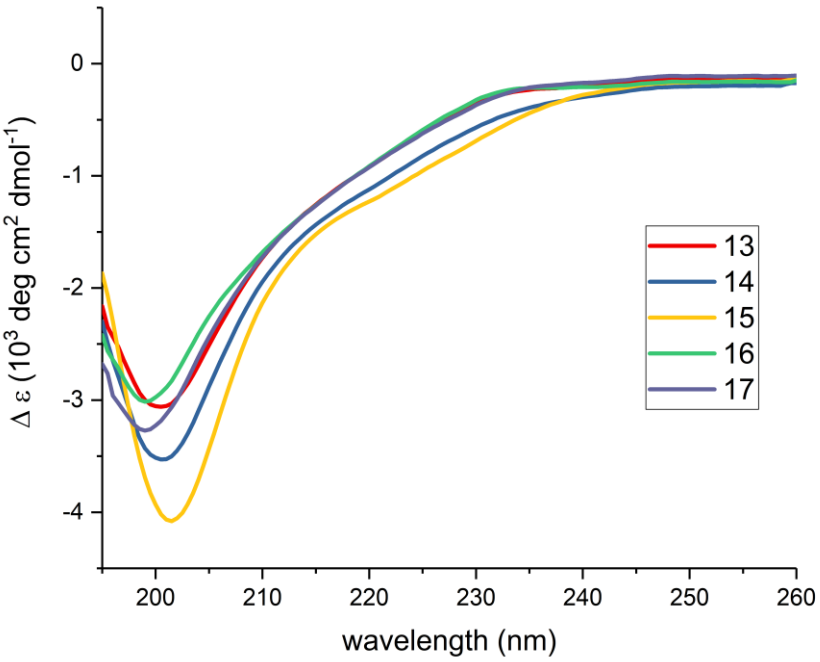

Figure S2-4. CD Spectra for (3-68) RANTES analogs **13**-**17**.

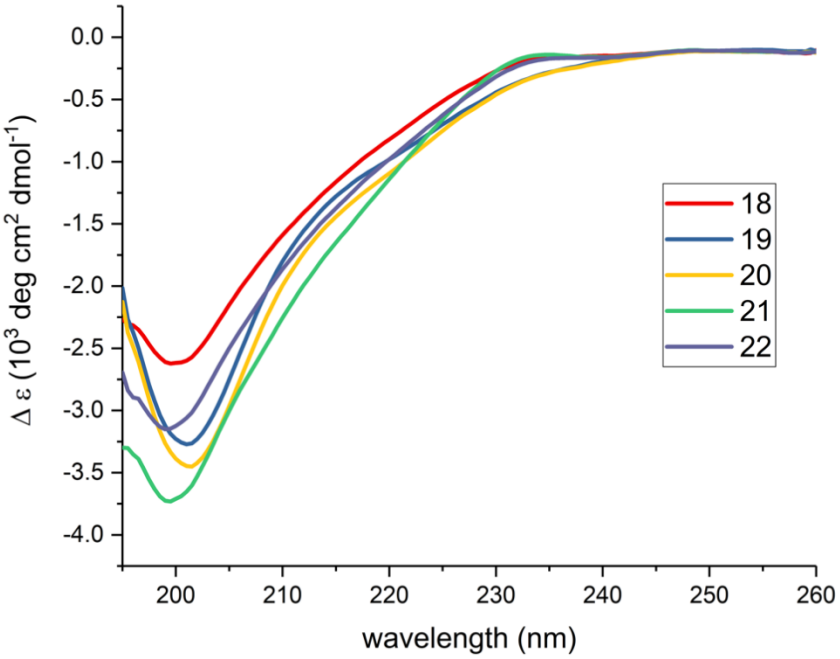

Figure S2-5. CD Spectra for (4-68) RANTES analogs **18**-**22**.

III. THP-1 cell migration

Table S1. Chemotactic index data for RANTES glycoforms **8**-**22**.

Glycoform		Chemotactic Index (CI)
8	(1-68)	1.000 ± 0.077
9	(1-68) S4G	0.278 ± 0.171
10	(1-68) S4GG	0.141 ± 0.090
11	(1-68) S5G	0.212 ± 0.068
12	(1-68) S5GG	0.072 ± 0.033
13	(3-68)	0.151 ± 0.077
14	(3-68) S4G	0.459 ± 0.160
15	(3-68) S4GG	0.000 ± 0.049
16	(3-68) S5G	0.309 ± 0.083
17	(3-68) S5GG	0.000 ± 0.027
18	(4-68)	0.053 ± 0.113
19	(4-68) S4G	0.025 ± 0.053
20	(4-68) S4GG	0.368 ± 0.112
21	(4-68) S5G	0.089 ± 0.018
22	(4-68) S5GG	0.000 ± 0.029

IV. Binding affinity of RANTES variants towards heparin

Table S2. Relative GAG binding affinity for RANTES glycoforms **8**-**22**, as measured by percent sodium chloride required to elute from a heparin-Sepharose column.

Glycoform		% NaCl required for elution	[NaCl] required for elution (mol L^{-1})
8	(1-68)	51.20 ± 0.26	1.024 ± 0.005
9	(1-68) S4G	49.27 ± 0.06	0.985 ± 0.001
10	(1-68) S4GG	47.77 ± 0.06	0.955 ± 0.001
11	(1-68) S5G	49.37 ± 0.06	0.987 ± 0.001
12	(1-68) S5GG	47.40 ± 0.10	0.948 ± 0.002
13	(3-68)	53.10 ± 0.10	1.062 ± 0.002
14	(3-68) S4G	50.30 ± 0.10	1.006 ± 0.002
15	(3-68) S4GG	48.57 ± 0.06	0.971 ± 0.001
16	(3-68) S5G	51.93 ± 0.21	1.039 ± 0.004
17	(3-68) S5GG	49.03 ± 0.12	0.981 ± 0.002
18	(4-68)	53.33 ± 0.06	1.067 ± 0.001
19	(4-68) S4G	49.90 ± 0.00	0.998 ± 0.000
20	(4-68) S4GG	48.80 ± 0.10	0.976 ± 0.002
21	(4-68) S5G	50.63 ± 0.06	1.013 ± 0.001
22	(4-68) S5GG	47.90 ± 0.10	0.958 ± 0.002

Table S3. Quantitative GAG binding affinity for RANTES glycoforms **8**-**22**, as measured by binding to fluorescently labeled heparin hexamers. * indicates no binding observed.

Glycoform		Kd (μM)
8	(1-68)	8.53 ± 0.71
9	(1-68) S4G	4.57 ± 0.33
10	(1-68) S4GG	29.15 ± 4.69
11	(1-68) S5G	16.55 ± 0.52
12	(1-68) S5GG	*
13	(3-68)	11.85 ± 0.40
14	(3-68) S4G	9.71 ± 0.69
15	(3-68) S4GG	8.42 ± 0.35
16	(3-68) S5G	39.97 ± 2.14
17	(3-68) S5GG	38.24 ± 2.33
18	(4-68)	19.32 ± 2.28
19	(4-68) S4G	6.74 ± 0.37
20	(4-68) S4GG	6.77 ± 0.47
21	(4-68) S5G	42.06 ± 7.71
22	(4-68) S5GG	24.66 ± 2.64

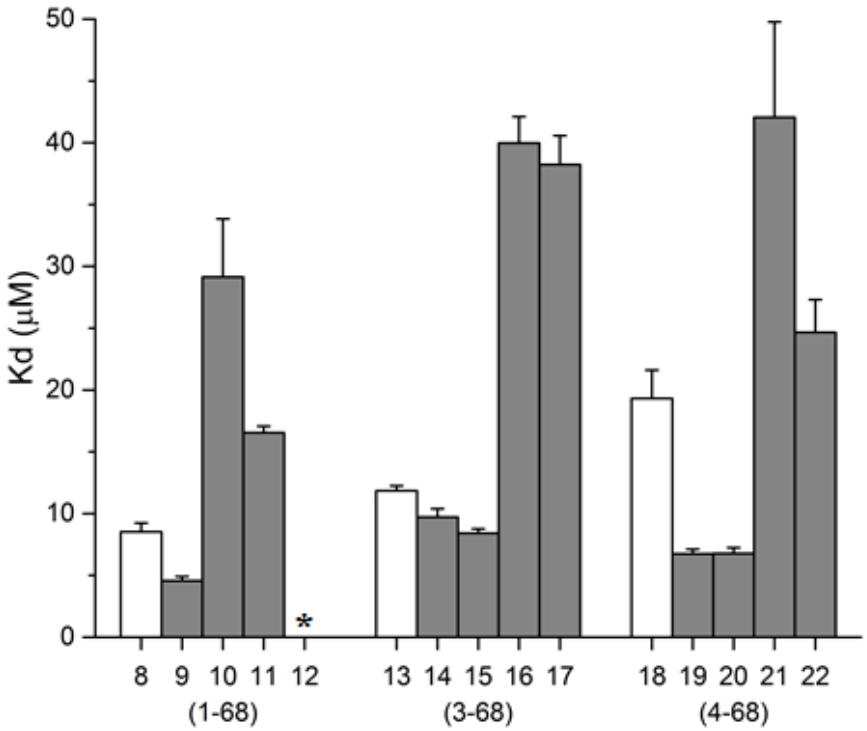

Figure S3. Quantitative GAG binding affinity for RANTES glycoforms **8**-**22**, as measured by binding to fluorescently labeled heparin hexamers. * indicates no binding observed.

V. Analytical ultracentrifugation of RANTES variants.

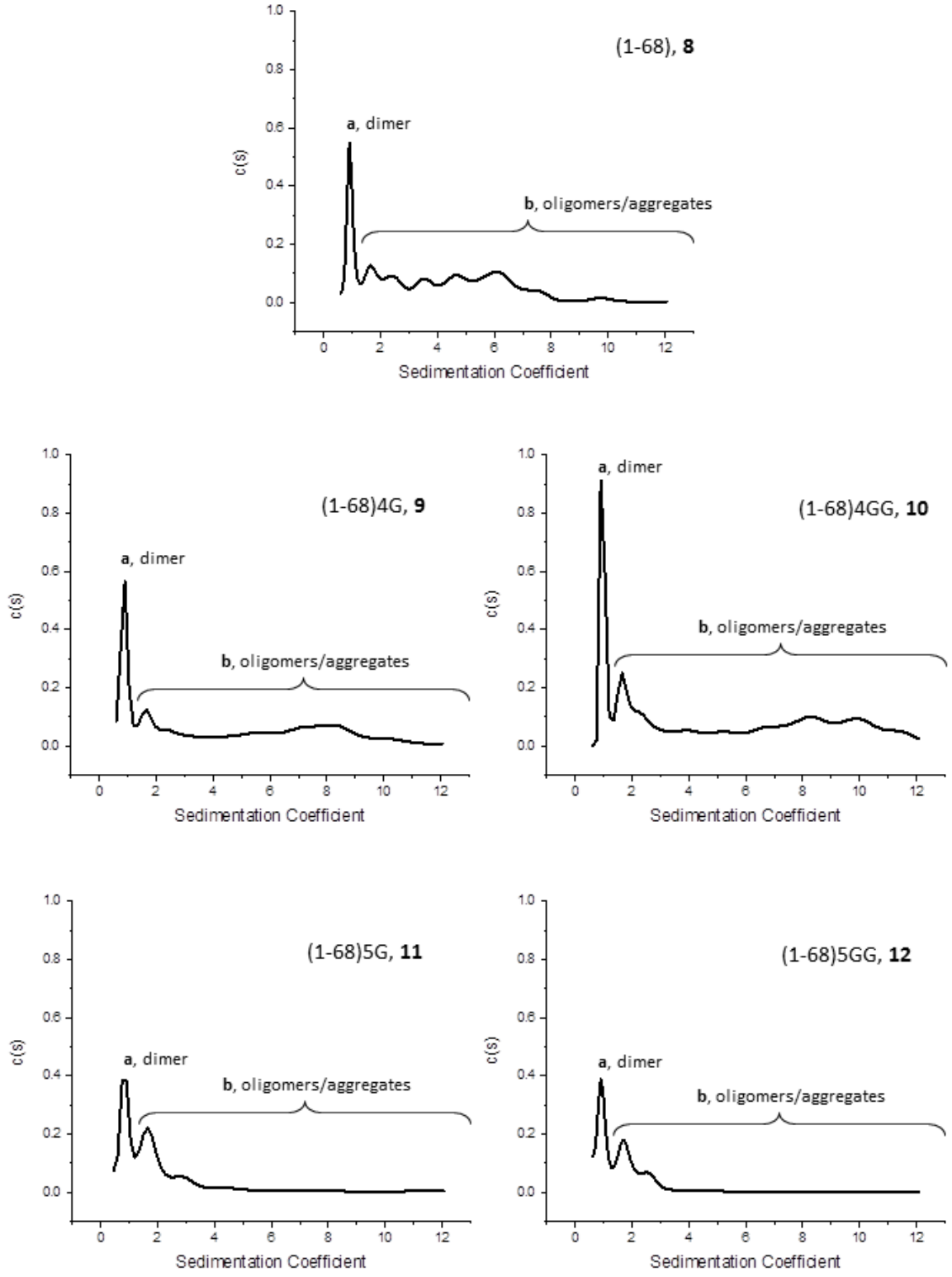

Figure S4-1. AUC traces for (1-68) RANTES analogs **8**-**12**.

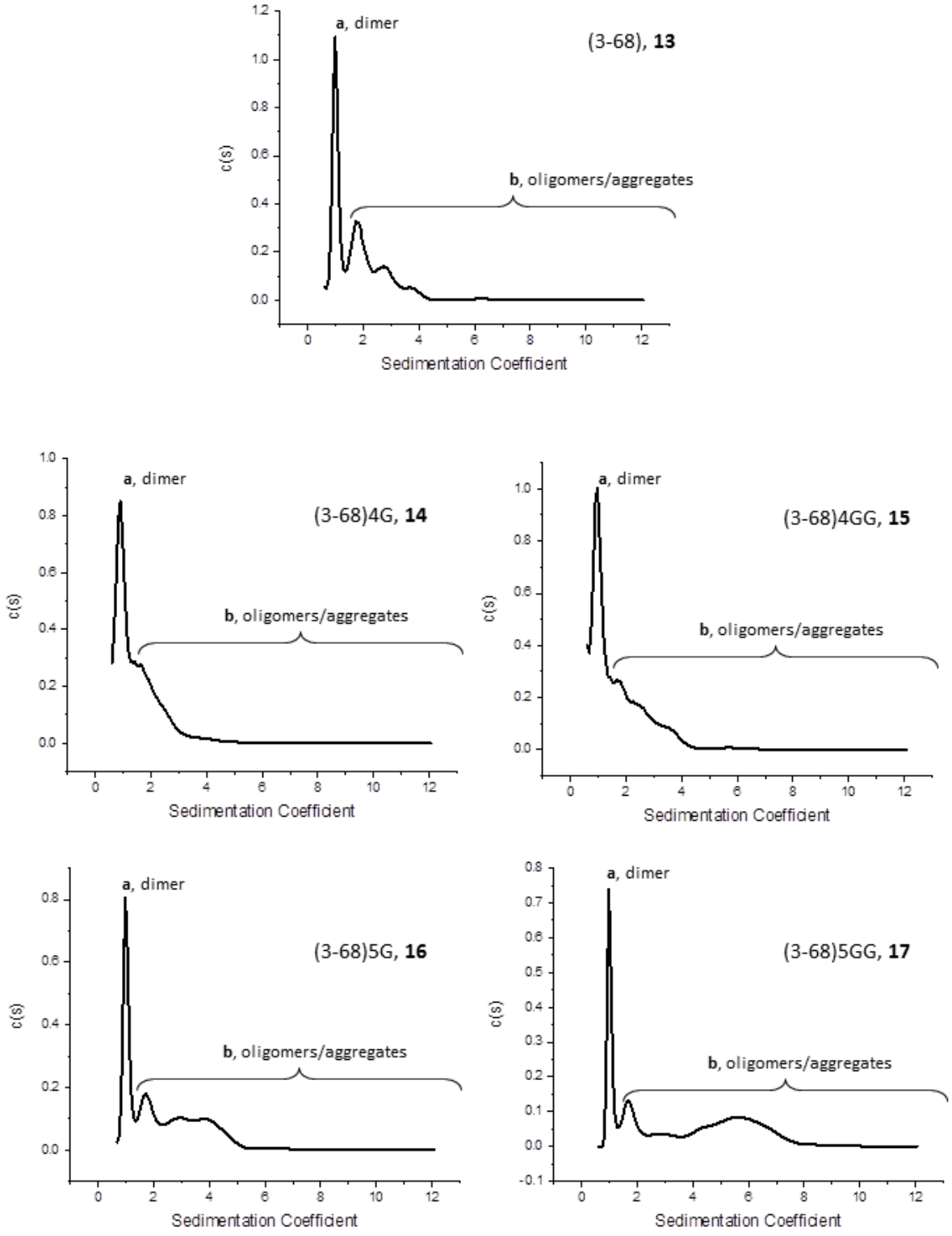

Figure S4-2. AUC traces for (3-68) RANTES analogs **13**-**17**.

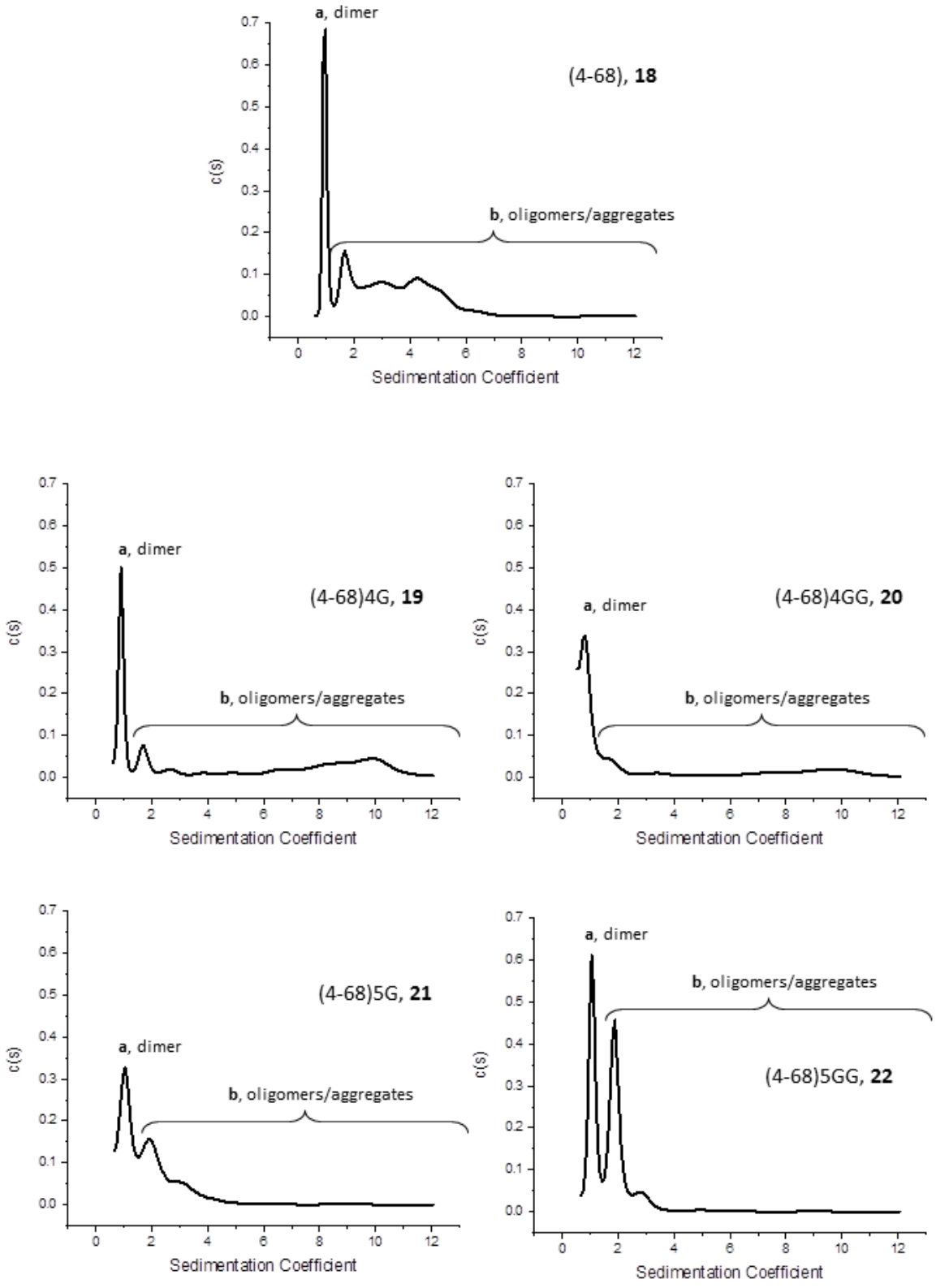

Figure S4-3. AUC traces for (4-68) RANTES analogs **18**-**22**.

VI. Inhibition of HIV-1 infection.

Table S4. Ability of RANTES glycoforms **8**-**22** to inhibit HIV infection. T-test compares each glycovariant to unglycosylated, full-length RANTES **8** (* indicates $p < 0.05$).

Glycoform		EC50 (μM)	p (probability associated with t-test)
8	(1-68)	0.016 ± 0.003	
9	(1-68) S4G	0.356 ± 0.028	0.035*
10	(1-68) S4GG	0.313 ± 0.247	0.339
11	(1-68) S5G	0.293 ± 0.029	0.045*
12	(1-68) S5GG	0.908 ± 0.704	0.324
13	(3-68)	0.006 ± 0.004	0.087
14	(3-68) S4G	0.060 ± 0.006	0.035*
15	(3-68) S4GG	0.050 ± 0.030	0.350
16	(3-68) S5G	0.512 ± 0.136	0.122
17	(3-68) S5GG	0.511 ± 0.315	0.269
18	(4-68)	0.073 ± 0.001	0.006*
19	(4-68) S4G	1.063 ± 0.187	0.080
20	(4-68) S4GG	1.839 ± 1.295	0.296
21	(4-68) S5G	2.370 ± 2.214	0.374
22	(4-68) S5GG	2.888 ± 1.774	0.262

VII. NMR study of RANTES variants

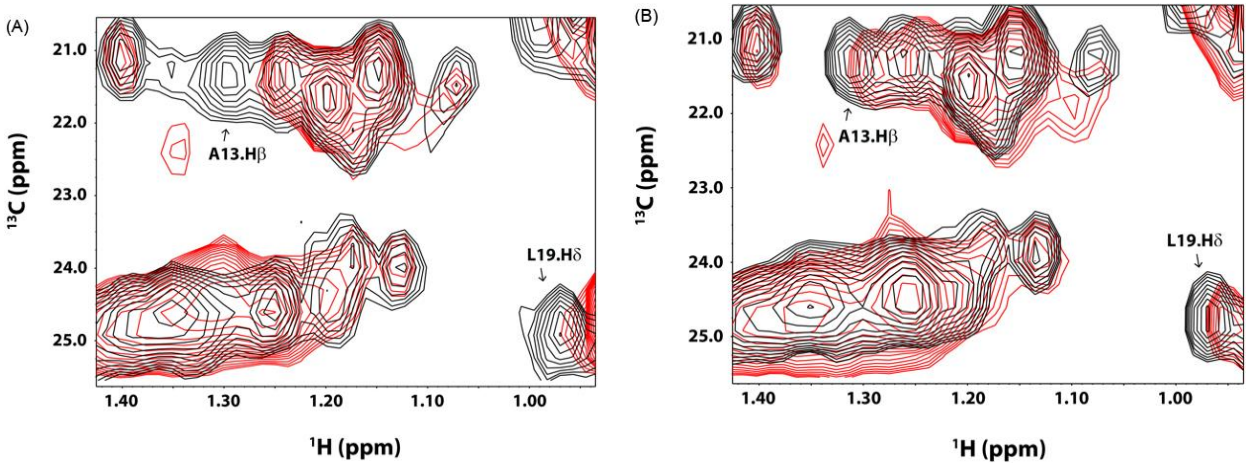

Figure S5. ^{13}C HSQC spectral changes induced by glycosylation in (A) RANTES (1-68) and (B) RANTES (3-68). Unglycosylated RANTES spectra shown in black color, glycosylated S4GG RANTES spectra shown in red color. Glycosylation induced small but significant changes in the positions of peaks. Interestingly, the truncated RANTES (3-68) exhibited less perturbation than the wild type protein.

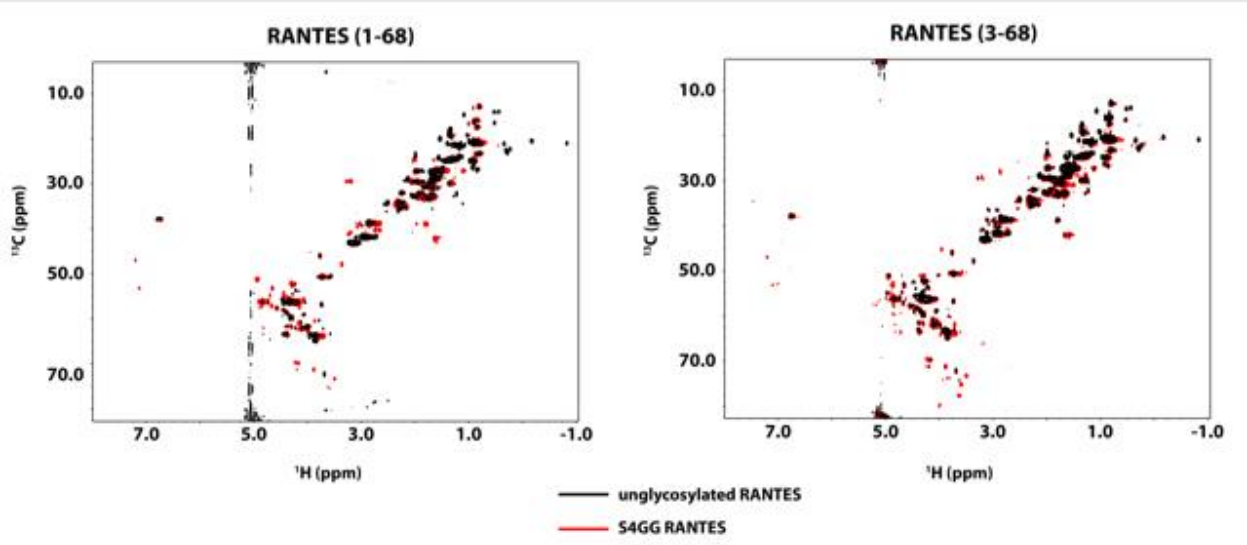

Figure S6. ^{13}C HSQC spectra for unglycosylated full length (1-68) RANTES and truncated (3-68) RANTES compared with the respective glycosylated analogs. RANTES samples 4 mg/mL in 20 mM ^{2}H-acetate buffer in D_2O, pH 4.5.